International Journal of Intelligent Transportation Systems Research
https://doi.org/10.1007/s13177-025-00556-y

Development of a Social Force Simulation Model for Mixed Vehicular Traffic at Roundabouts

Salma Abo-Bakr[1] · **Karim Ismail**[2] · **Mohamed El Esawey**[1] · **Mostafa H. Tawfeek**[1]

Received: 13 May 2025 / Revised: 16 September 2025 / Accepted: 18 September 2025

Abstract

In recent decades, the simulation of vehicular traffic at roundabouts has received notable attention among traffic professionals. Developing reliable tools, specifically to model roundabout traffic, is vital given the growing interest in analyzing roundabout traffic operation and safety. These tools can play an important role in anticipating the effectiveness of any traffic design and control change at roundabouts. The social force-based model (SFM) has been widely used in simulating the movements of road users and their interactions at different traditional and shared space zones. Despite their strengths, SFMs have not been applied to simulate the movements and interactions of vehicles at traditional or even shared-space roundabouts. This study proposes an SFM for the movement of mixed vehicular traffic at traditional roundabouts. The calibration and validation of the model were undertaken using open trajectory datasets from a roundabout in Germany. The local transferability of the model was tested using datasets from other locations in Germany. The results showed that the calibrated model could replicate different traffic movements at the roundabout. Moreover, the calibrated model showed good performance in terms of the root mean square error (RMSE) of predicted vehicle trajectories and speeds, final destination error (FDE), and average distance error (ADE) when applied at other locations in Germany. The RMSE of trajectory and speed, ADE, and FDE from using the validation dataset were 0.35 m, 0.19 m/sec, 0.26 m, and 0.57 m, respectively. The external transferability of the model to another environment in a different country was further explored where the model parameters were re-calibrated using trajectory data from a roundabout in the USA. From the comparison between the calibrated values of each parameter, it was concluded that five of the eleven common calibrated parameters are transferable, while the other parameters should be re-calibrated to improve the performance of the model at different locations. Finally, it was concluded that the proposed model can depict the movement of different vehicles at the roundabout after proper calibration for the non-transferable parameters.

Keywords Social Force Microsimulation Model · Mixed Traffic · Model Calibration · Transferability · Roundabout

1 Introduction

Traffic micro-simulation tools play a vital role in traffic engineering because they facilitate evaluating the current traffic situation, predicting outcomes of new control systems, and new infrastructure designs [1–4]. The available models are designed to replicate homogeneous traffic with strong lane discipline, where the characteristics of vehicles and their behavior are nearly the same. Therefore, modeling heterogeneous traffic, especially under weak-lane discipline where there is a diversity in the road users and their behavior, dimensions, and operational characteristics, is considered a challenge to traffic engineers. Similarly, modeling the traffic at roundabouts is considered a challenge because the vehicles' movements differ from road segments due to the various movements at exits, entries, and circulating segments. In other words, vehicles approaching the roundabout from different entries must yield and select their route to exit the roundabout from various exits through continuous merging and diverging, facing random interactions with other vehicles and road geometry. Therefore, traffic at

✉ Salma Abo-Bakr
salma.hussein@eng.asu.edu.eg

[1] Department of Civil Engineering, Ain Shams University, Cairo 11517, Egypt

[2] Department of Civil Engineering, Carleton University, Ottawa K1S 5B6, Canada

Published online: 29 October 2025

roundabouts is complex, and commercial micro-simulation tools may struggle to capture it.

Traditional roundabouts differ from shared spaces in terms of the design, traffic composition, and control. Traditional roundabouts are characterized by defined, clear right-of-way, traffic control systems to manage the movement of vehicles, and the presence of crosswalks for pedestrians. Sometimes, traffic engineers add separate lanes for bicycles or other vulnerable road users. In contrast, in shared spaces, non-motorized vehicles such as bicycles and e-bikes share the same road space with pedestrians or motorized vehicles, and the movements and interactions of the road users are based on informal social and priority negotiation [5, 6]. This encourages vehicles to reduce their speed and increase awareness, which in turn improves traffic safety. Moreover, the design of the shared spaces includes the removal of traffic signals, lane markings, barriers, and curbs [6].

Physical-based models, such as the social force model (SFM), have been widely adopted to model traffic with interactions between various road users and their movements in different contexts [7–12]. It could be considered that SFM can manage the movement of vehicles and their interactions with each other and the road geometry at complex systems like roundabouts [13]. Despite its strength, the concept of SFM has not been applied to model vehicular traffic at roundabouts, where motorized vehicles dominate, compared to other two- and three-wheeler vehicles. As such, this study aims to develop a microscopic SFM to simulate vehicles' movement and interactions at multi-lane roundabouts. The study also addressed the calibration of the SFM parameters to replicate the local behavior at the studied roundabouts. The validation of the calibrated model was conducted using a trajectory dataset from Germany. The potential transferability of the calibrated model to other similar locations in Germany, as well as to a roundabout in the USA, as an example of another driving environment, is investigated. The similarity between the simulated and the real-life trajectories was assessed, and the transferable parameters were specified.

2 Literature Review

Roundabouts are considered an efficient and safe alternative compared to stop-sign control and signalized intersections [14–16]. Therefore, it is essential to find a model that could successfully simulate the traffic at roundabouts to analyze their operations and safety. The following subsections mention the previous studies that modeled different roundabouts using various techniques, in addition to the application of social-force-based theory in simulating the dynamics of road users at different zones.

2.1 Modeling Traffic at Roundabouts

Various models have been utilized to model vehicle dynamics at traditional and shared-space roundabouts such as commercial microsimulation tools, cellular automata (CA), and social force models (SFM). Commercial traffic microsimulation tools are based on integrated car-following and lane-changing models but depend on extensive calibration of the model parameters. These models have been used extensively to model traffic at roundabouts. For example, Li et al. [17] proposed procedures for modeling and calibrating roundabouts in VISSIM. However, they validated the recommendations using data from one roundabout and did not discuss their transferability to other study sites. Giuffrè et al. [18] used VISSIM and SSAM to compare the efficiency and the safety performance of standard roundabouts and new layouts. Moreover, car-following models were calibrated and applied to model car-following behavior at roundabouts and intersections [19]. The models' parameters were calibrated using real-life data without validation, and the lateral movements of vehicles and their interactions were not considered. Finally, modeling roundabouts in VISSIM requires defining the reduced speed areas and analyzing the performance of the two right-of-way options, priority rule or conflict area, before simulation to find which one reflects the observed traffic behavior [17]. Also, numerous parameters of the driving behavior models should be calibrated to mimic the local conditions.

Many studies have been carried out to compare microsimulation tools for modeling roundabouts. For example, SUMO was compared to VISSIM and TRANSIMS in simulating roundabouts, and SUMO showed unrealistic results [20]. Multiple roundabouts in the U.S. were modeled using RODEL and SIDRA. No single model was shown to be the best in terms of all the evaluation measures used [21]. Nikolic et al. [22] simulated single-lane and multi-lane roundabouts using AIMSUN, PARAMICS, VISSIM, SIDRA, NCHRP, RODEL, and ARCADY and found that AIMSUN and VISSIM provided the best results compared to other models. From the comparative studies, there was no single microsimulation tool that could accurately describe the movements and interactions at roundabouts.

On the other hand, Cellular Automata (CA) is a rule-based model which divides the road space into discrete cells of a specific width, and each cell is either empty or occupied by a vehicle. The vehicles change in their positions through defined transition rules, i.e., acceleration or deceleration [23]. Studies have applied the CA models to represent the traffic at single-lane roundabouts [24–27]. Other studies have considered the traffic at normal and large multi-lane roundabouts using the CA model [28–33]. The complex interactions between vehicles at large multi-lane

roundabouts were also captured using CA [34, 35]. The previous studies have shown that different CA models could successfully model traffic at different roundabouts based on clearly defined transition rules. However, it is not easy to set clear rules in the presence of various vehicle types with continuous interactions due to the discrete nature of the CA [36]. Moreover, the accuracy of the CA model depends on the size of the cells; the accuracy increases with further spatial division into smaller cells, but it is not feasible to divide the road environment into infinitely small cells.

2.2 Micro-simulation Using SFM

The SFM is a spatially continuous model that was first introduced to simulate pedestrian motion by Helbing in 1995 [37]. Road users continuously update the magnitude and direction of their speed and direction at any time based on the resultant social forces acting on them, while aiming to reach their destinations and avoiding collisions with other users and obstacles. Unlike traditional car-following and lane-changing models, SFMs can imitate the lateral interactions between different modes under mixed traffic. Therefore, the notion that road users exert social forces on each other while interacting has been adopted to mimic the behavior of different road users and their interactions in different road zones under mixed traffic. It was mainly introduced by Helbing to model pedestrian movements; however, Fellendorf et al. [38] have initiated the application of SFM to describe the dynamics of cars in a two-dimensional environment with no lanes defined. After that, SFM has been applied to model the interactions between cars and pedestrians in shared spaces (Anvari et al., 2016). Moreover, SFMs were extended to capture the movements of other motorized and non-motorized vehicles. For example, models were developed to describe the interactions between pedestrians and personal mobility vehicles (PMVs) on a shared sidewalk [8]. It has been used to model the movement of bicycles [11, 12], and their interactions with pedestrians and cars in shared spaces [39–42]. As well, the SFM was used to simulate the behavior of motorcyclists under mixed traffic [40, 41], and the behavior of electric bikes in mixed traffic along a segment in China [43].

In recent studies, Johora and Müller [7, 44, 45] proposed a multi-agent-based simulation model that could represent multiple interactions between pedestrians and cars in shared space zones such as streets, unsignalized intersections, and roundabouts. They calibrated and validated the model using real-life data from shared spaces in Germany and Austria, in addition to addressing its transferability using data from China. They concluded that the model could be applied to various shared spaces in any context after some modifications [46]. It is noteworthy that the used dataset was collected from a roundabout on a university campus which included trajectories of many pedestrians and fewer vehicles. Moreover, the study focused on many car-to-multiple-pedestrians crossing scenarios. Moreover, the SFM was used to imitate the behavior of vehicles and their interactions at urban signalized intersections in China with diverse types of work zones, e.g., an island work zone [47] and straddling work zones [48]. These studies included driving force, repulsive force with other vehicles and boundaries, passable gap force, and following force, and validated the model's efficiency in capturing traffic under heterogeneous traffic using real data.

In summary, several studies have been undertaken to model traffic at roundabouts using different techniques. Nevertheless, it is evident that the SFM has never been applied to simulate vehicular traffic at roundabouts with only one exception where it was used to model the crossing behavior of pedestrians and their interactions with cars at shared-space roundabouts [46]. Furthermore, only a few studies have examined the suitability of SFM in modeling different vehicular road users in traditional road facilities, while none of them have analyzed traditional roundabouts. Traffic movements at roundabouts are continuous, which makes them suitable to be modeled using continuous models such as SFM rather than discrete rule-based models such as CA models. Moreover, it has proved efficient in capturing the behavior of various vehicular road users and their interactions under different shared spaces, in addition to the interactions between cars and pedestrians' crossings at traditional intersections. As such, this study aims to develop a SFM to simulate vehicular traffic movements at roundabouts. Additionally, the study aims to calibrate the proposed model and examine its transferability to other locations.

3 Simulation Modeling Framework

Figure 1 shows the framework of the developed simulation model based on the SFM. As a first step, data on the geometry of the roundabout and the positions, velocities, and destinations of all vehicles are defined. In the next step, a free-flow path is specified for each vehicle. At each time step (t), obstacles and other vehicles within the field of view (FoV) of the agent (i) and its next destination are determined. Finally, the social forces acting on the subject vehicle (i) at time (t) are computed to determine its new position and velocity at the next time step (t+1). At the end of each time step, the model checks whether the subject vehicle has reached their final destination. If the destination has not been reached yet, the model will consider its new state in the next time step. The following sub-sections explain the model in greater detail.

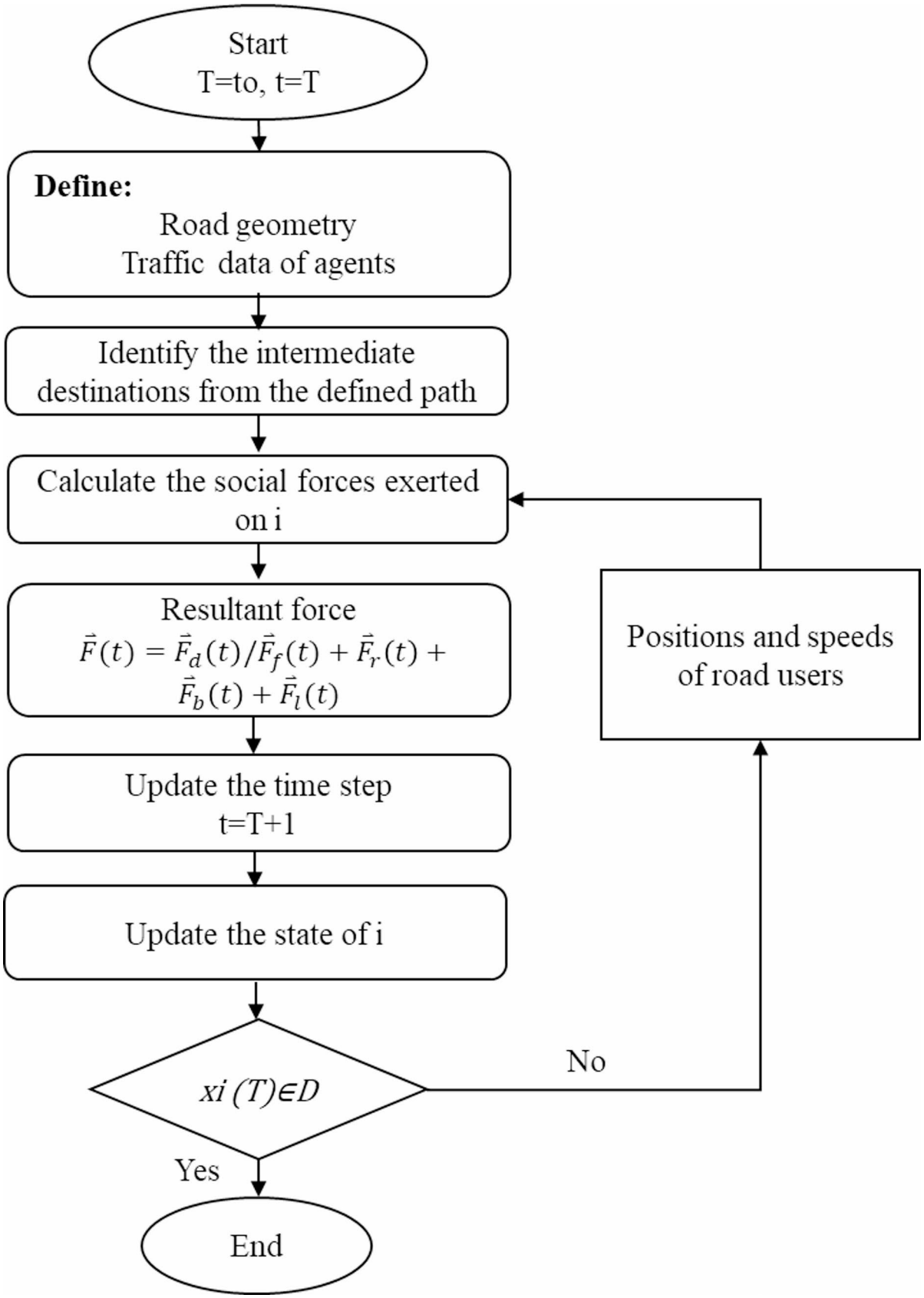

Fig. 1 The framework of the developed SFM at roundabouts

3.1 Free-Flow Trajectory Planning

To guide the vehicle during the simulation, it is not sufficient to take the final destination as the target position [38]. Therefore, intermediate destinations are set on a predefined path between the origin and the destination for each agent. These paths are determined before the beginning of the simulation, considering only the static obstacles. Generally, different path planning algorithms were used in the literature, such as the flood fill algorithm [49, 50], A* [7, 44], and the Dijkstra algorithm [41]. In this study, the Hybrid A* algorithm was selected for the path-planning process [51, 52] using the navigation toolbox in MATLAB. The Hybrid A* algorithm considers vehicle dynamics and kinematics, and it overcomes the limitations of the traditional A* algorithm, where only the cells' centers can be visited [53, 54]. As shown in Fig. 2, the A* algorithm only visits states that correspond to the cell centers, while the Hybrid A* algorithm associates a continuous state with each cell. Hybrid A* produces a drivable path that is safe, smooth, and satisfies the turning radius of the vehicle. The main inputs for the path planning step for each vehicle movement are a grid map, the initial state, and the goal state of the vehicle. For each studied roundabout, a path was planned for each movement in the roundabout. Figure 3 shows an example of the planned path by the algorithm for one movement generated from MATLAB.

3.2 The Social Force Model for the Traffic Flow of Vehicles

The proposed model adopted five social forces, including the classical SFM forces and other forces for describing the following and lane discipline behavior of various vehicles. These five forces describe the movements and interactions of vehicular road users at a roundabout as discussed below.

3.2.1 Driving Force $\vec{F}_d$

This force allows the vehicle (i) to adopt a desired speed at each time step within a relaxation time until it reaches its final destination. The value of the force depends on the difference between the actual speed and the maximum allowable speed, as shown in Eq. (1).

$$\vec{F}_d = \frac{v_d * \vec{e}(t) - \vec{v}_t^i}{t_r} \tag{1}$$

where v_d is the desired speed which is obtained from the real-life data for each vehicle type, $\vec{v}_t^i$ is the current velocity of the object (i) at time (t), t_r is the relaxation time and has different values based on the vehicle class, and $\vec{e}(t)$ is the unit vector pointing from the subject vehicle along the shortest path to its destination at time (t).

3.2.2 Repulsive Force with other vehicles $\vec{F}_{vij}$

A vehicle tends to keep safe distances from nearby vehicles within its field of view (FOV). As such, a repulsive force is acted on vehicle (i) by other agents (j) to avoid collision. The value of this repulsive force increases exponentially when the distance between vehicles increases, as expressed below.

$$\vec{F}_{vij} = \left(A_r * e^{\left(\frac{r_{ij}-d_{ij}}{B_r}\right)} * \vec{n}_{ij}\right) * FoV_{ij} \tag{2}$$

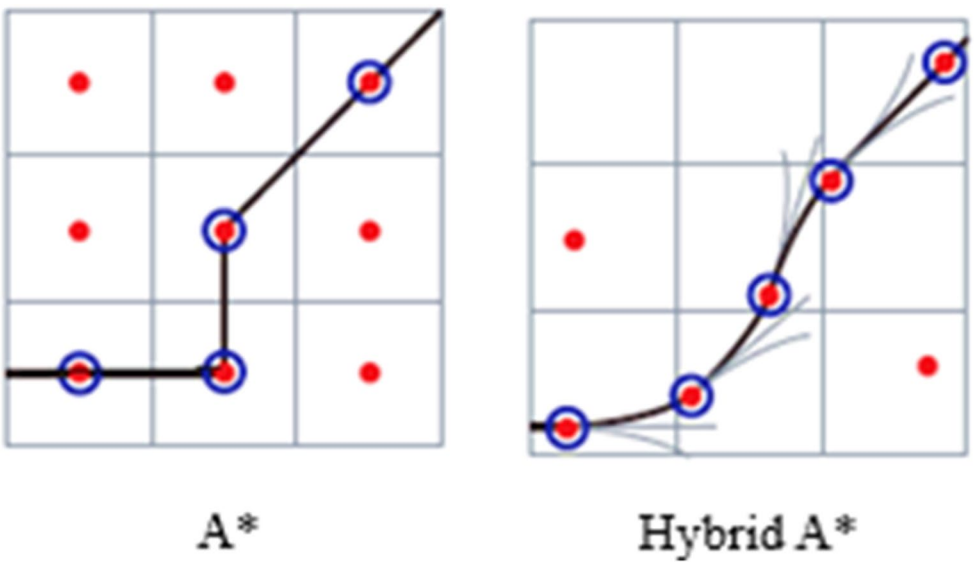

Fig. 2 A comparison between the path planning algorithms (A* and Hybrid A*) [51]

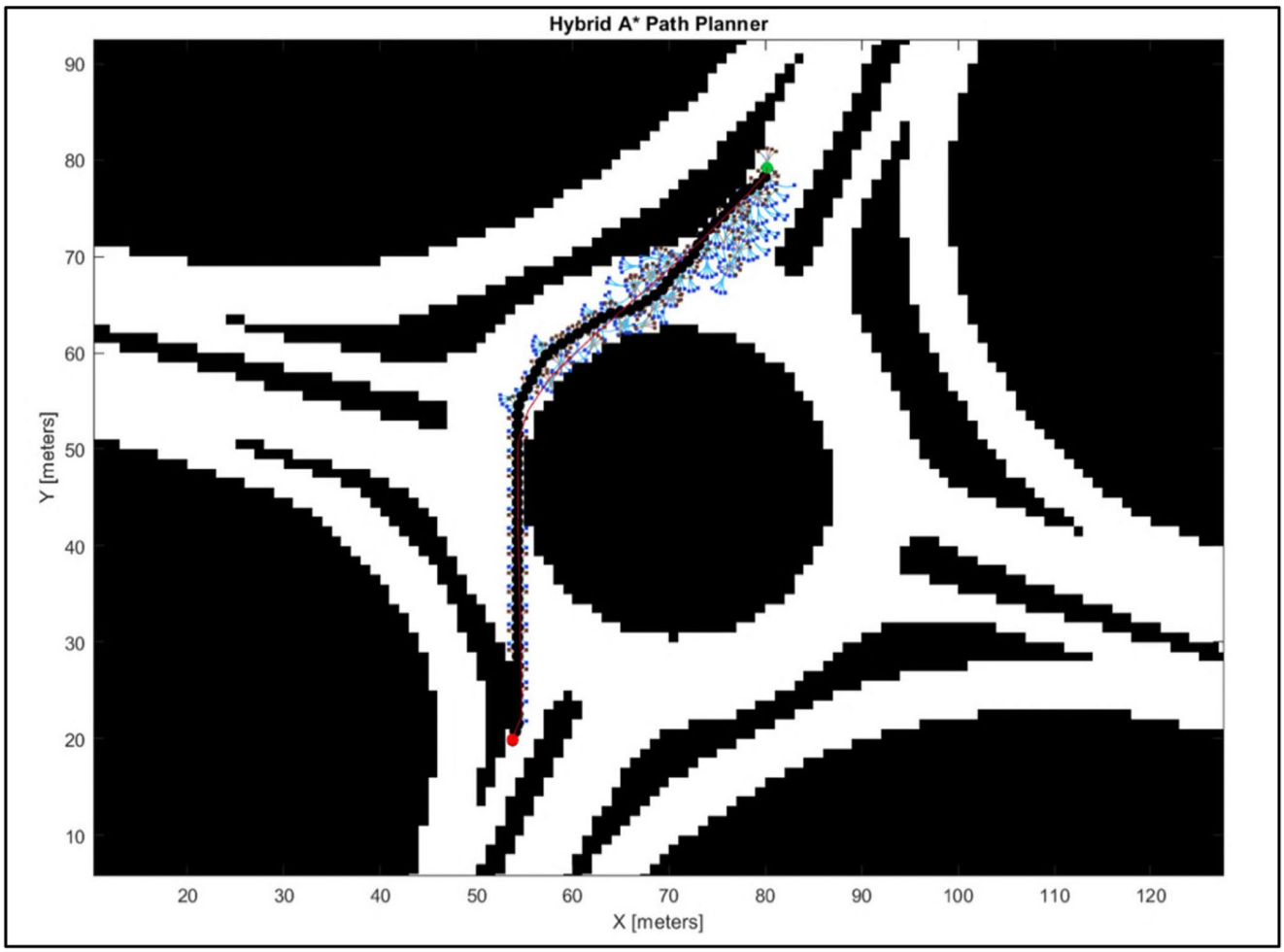

Fig. 3 An example of the planned path using a Hybrid A* algorithm

where A_r is the interaction strength for the force (m^2/sec^2), B_r is the acting range of the force of the vehicle j (m), d_{ij} is the distance between the centers of the two vehicles, r_{ij} is the sum of their radii and is computed using Eq. (4), $\vec{n}_{ij}$ is the normalized vector from (j) to (i), and FOV_{ij} is a factor representing the visible range (i) and is calculated using the following equation:

$$FOV_{ij} = \left(\lambda_i + (1-\lambda_i) * \frac{1+cos\left(\propto_{ij}\right)}{2}\right) * k \qquad (3)$$

where $\propto_{ij}$ is the angle between the movement direction of road user (i) and the direction of vehicle (j) and λ is an anisotropic factor ($0 \leq \lambda \leq 1$) which represents the strength of the force on the different nearby vehicles; this implies that the following vehicle affects the followed vehicle more than the one behind. q is a factor for the vehicle-vehicle interaction function as follows [55]:

$$k = \begin{cases} 1, if\ 150 \leq \propto_{ij} \leq 210\ and - 30 \leq \propto_{ij} \leq 30 \\ 0, \qquad otherwise \end{cases}$$

Rather than representing the pedestrian as a circle in the social force model [56], in this study, a vehicle is represented by an ellipse with radius $[r_i\left(\propto_{ij}\right)]$ [55], as illustrated in Fig. 4. This radius depends on the angle $(\propto_{ij})$ between the directions of (i) and (j) at time (t) and the vehicle class because it is a function of the vehicle's dimensions, as shown in Eq. (4).

$$r_i\left(\propto_{ij}\right) = \frac{w}{\sqrt{1-\epsilon^2 * cos^2\left(\propto_{ij}\right)}} \qquad (4)$$

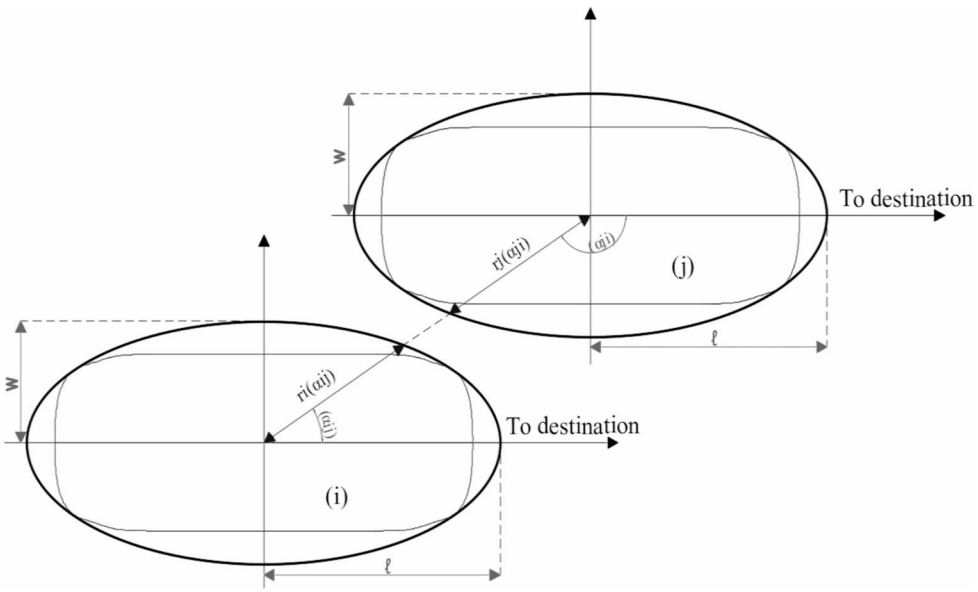

Fig. 4 Geometric modeling of the vehicle as an ellipse

where $\in = \frac{\sqrt{l^2-w^2}}{l}$, 2w and 2 L are the width and length of the vehicle (i), respectively, which vary depending on the vehicle class.

3.2.3 Repulsive Force from obstacles $\vec{F}_{bio}$

This force is exerted by the road boundary or any obstacle on the subject road user (i) to avoid colliding with the road boundary. This force makes the road user maintain a safe distance from any fixed obstacle. Similar to the repulsive force from other vehicles, this force depends on the distance between the agent (i) and the boundary and is formulated as follows:

$$\vec{F}_{bio} = A_{io} e^{\left(\frac{w-d_{io}}{B_{io}}\right)} * \vec{n}_{io} \tag{5}$$

where A_{io} is the interaction strength for the force (m^2/sec^2), B_{io} is the acting range of the force of the obstacle (m), w is half the width of the vehicle, and it depends on the vehicle class, d_{io} is the perpendicular distance between (i) and the boundary, and n_{io} is the unit vector directed from the obstacle (o) to the (i).

3.2.4 Lane-keeping Force $\vec{F}_{lil}$

It reflects the behavior of the lane discipline by exerting a force on the vehicle from the lane lines to keep it within the lane. It is calculated as shown in Eq. (6).

$$\vec{F}_{lil} = A_l e^{\left(\frac{w-d_{il}}{B_{il}}\right)} *_{\vec{n}_{il}} \tag{6}$$

where A_l donates the strength for the force (m^2/sec^2), B_{il} is the acting range of the force from the lane line (m), d_{il} is the distance between the vehicle (i) and the lane line, and $\vec{n}_{il}$ is a vector from the lane line to the center of the vehicle (i).

3.2.5 Following force $\vec{F}_f$

It represents the following behavior of the driver to avoid collision with the leading vehicle as long as the distance between the two vehicles is less than a spatial distance (d_{min}), and both have nearly equal directions [7, 55]. Gipp's car-following model was incorporated with SFM to handle the longitudinal interactions in case of following a leader vehicle (j). According to Eq. (7), it allows vehicle (i) to adopt a safe velocity (v_s) to follow the leading vehicle to keep a safe following distance through accelerating or decelerating or keeping its current speed based on the difference between its velocity at time (t) and the safe velocity.

$$\vec{F}_f = k * \left(\frac{(v_s - v_i(t))}{t_r} * \vec{n}_{ij} \right) \tag{7}$$

where $\vec{n}_{ij}$ is the unit vector directed from (i) to the preceding vehicle (j), v_s(t) is the safe velocity which the following vehicle should not exceed while following the leading vehicle at time (t), and is computed by Gipps' safety car-following model [57, 58], as shown in Eq. (8):

$$v_s = \sqrt{a_i^2 * {t_r}^2 + a_i\left(\frac{2 * g_{ij}(t) - t_r * v_i(t) + v_j^2(t)}{a_j}\right)} - a_i * t_r \tag{8}$$

where $a_i \, and \, a_j$ are the maximum deceleration rates of the following and leading vehicles, respectively, t_r is the relaxation time, $g_{ij}\,(t)$ is the gap between (i) and (j) at time (t), and $v_j\,(t)$ is the velocity of (j) at time (t). k-term is added to decide whether the following force is applied or not, depending on the distance between the two vehicles (d_{ij}), as follows:

$$k = \begin{cases} 1, if\ d_{ij} < d_{min} \\ 0\ , otherwise \end{cases}$$

3.2.6 Resultant forces and the determination of the new vehicle's state

At each time step (t), the resultant of the social forces acting on a subject vehicle (i) is computed and used to determine the new velocity and position at time (t+1) as follows:

$$\vec{v}_l\ (t+1) = \vec{v}_i\,(t) + \vec{F}\,(t) * \triangle t \tag{9}$$

$$\vec{x_l}\,(t+1) = \vec{x}_i\,(t) + \frac{1}{2} * \vec{F}\,(t) * \triangle t^2 + \vec{v}_i\,(t) * \triangle t \tag{10}$$

where $\vec{F}(t)$ is the resultant of the social forces acting on the vehicle (i) at time (t), $\Delta\, t$ is the time step, $\vec{v}_i(t+1)$ and $\vec{x}_i(t+1)$ is the state of the vehicle (i) at the next time (t+1).

4 Model Implementation

The proposed model was implemented in MATLAB with a finite simulation time step to assess the performance of different model scenarios in replicating the movements at roundabouts. The geometric design and the traffic data for different roundabouts were defined as model inputs. The traffic physical characteristics and speeds of each vehicle type were added to the model without any conversion to a passenger car unit (PCU). The output of the model includes the speeds and positions of each vehicle at each time step during the whole simulation period. The data used for the study and the applied calibration methodology are described below.

4.1 Data Description

Two different trajectory datasets from roundabouts in two different countries were used to examine the model's performance. The first dataset was the RounD dataset which includes trajectories of different road users recorded in Germany [59]. The trajectories were extracted from more than six hours of drone recordings at three different roundabouts in and around Aachen in the western part of Germany, as shown in Fig. 5. A description of each location is given below [60]:

- Location 1 connects a highway with Aachen, all the entries are two lanes, and the exits are one lane [Fig. 5 (a)]. Most of the recordings were for this site because it has the highest traffic volume.
- Location 2 is located in an urban area in Aachen and connects a ring road with smaller roads leading to the city [Fig. 5 (b)]. All the entries and exits are single-lane.
- Location 3 is a less frequented roundabout located in the suburb of Aachen with a single lane at each entry and exit [Fig. 5 (c)].

The data collected included trajectories from three locations of a total of 13,476 vehicles of various types, including cars, buses, trailers, trucks, vans, and vulnerable road users (VRU) (motorcycles and bicycles). The data included x-y positions, x-y velocities and accelerations, vehicles' length and width, frame numbers, and vehicle class of each tracked object at 25 frames per second (fps). These data were used for model calibration, validation, and transferability. Data from Location 1 (ID1) were used for the calibration and validation of the model. The calibration dataset included trajectories of almost 18 min, while the validation data included two other subsets from the same location of nearly 18 and 17 min, respectively. The performance of the validated model was further tested using trajectory data from the other two locations to check the transferability of the model parameters to other locations in the same country (i.e., local transferability). Although all the roundabouts are located in Aachen, they have different numbers of lanes, different traffic volume patterns, and are located in different areas of the city. For instance, Location 2 (ID2) has through, left-turn, and right-turn at all approaches similar to the intersection used for calibration (ID1), while there were no right turns at the third roundabout (ID3). For instance, the real trajectories of a car and a bicycle (as an example of a VRU) are represented in Fig. 6 to show their movements and interaction at the roundabout. Both were driving across the roundabout at the same time.

The second dataset was a trajectory-based dataset from the USA. The dataset is known as the "UCF SST CitySim DataSets" collected at a multi-lane roundabout in Florida, USA [61, 62], as shown in Fig. 7. The roundabout connects a four-lane divided road with a two-lane two-way road. The trajectories were extracted from five drone video recordings captured at 30 fps for two hours. The data included

Neuweiler, Aachen (ID1)

(b) Kackertstraße, Aachen (ID2)

(c) Thiergarten, Alsdorf (ID3)

Fig. 5 Layout of the three roundabouts from Germany [59]. Neuweiler, Aachen (ID1).(**b**) Kackertstraße, Aachen (ID2). (**c**) Thiergarten, Alsdorf (ID3)

trajectories, velocities, and frame IDs for each vehicle at each time step.

Unlike the roundabouts in Germany, the traffic at the USA location included only passenger cars. The external transferability of the model was examined using trajectories of a 20-minute video from this dataset. This case represents a roundabout from another country with different geometry and traffic flow characteristics. Table 1 summarizes the attributes of each dataset used in the study.

4.2 Model Selection

As explained in Eqs. (9) and (10), the state of the vehicle at time step (t+1) depends on the state at time step (t) and the resultant of the social forces acting on the vehicle. Traditionally, all five discussed forces are added to compute the state of the vehicle. However, this study investigated the performance of different combinations of forces, as well as considering all the forces together. For instance, in the case of a Following Force exerted from vehicle (j) on the subject vehicle (i), it is added to the classical forces (i.e., Driving Force and Repulsive Force from vehicles and boundaries) when computing the vehicle's new state in the previous studies. The Following Force enforces the vehicle to maintain a safe velocity to follow the leading vehicle. This raises two questions: (1) Does the Safe Velocity force keep the following vehicle at a safe distance from the leading vehicle, and, in this case, can the Repulsive Force from the leading vehicle be ignored? (2) Will the following vehicle change its speed to achieve the safe speed? Additionally, can the Driving Force, which makes the vehicle adopt a desired speed to reach its destination, be ignored?

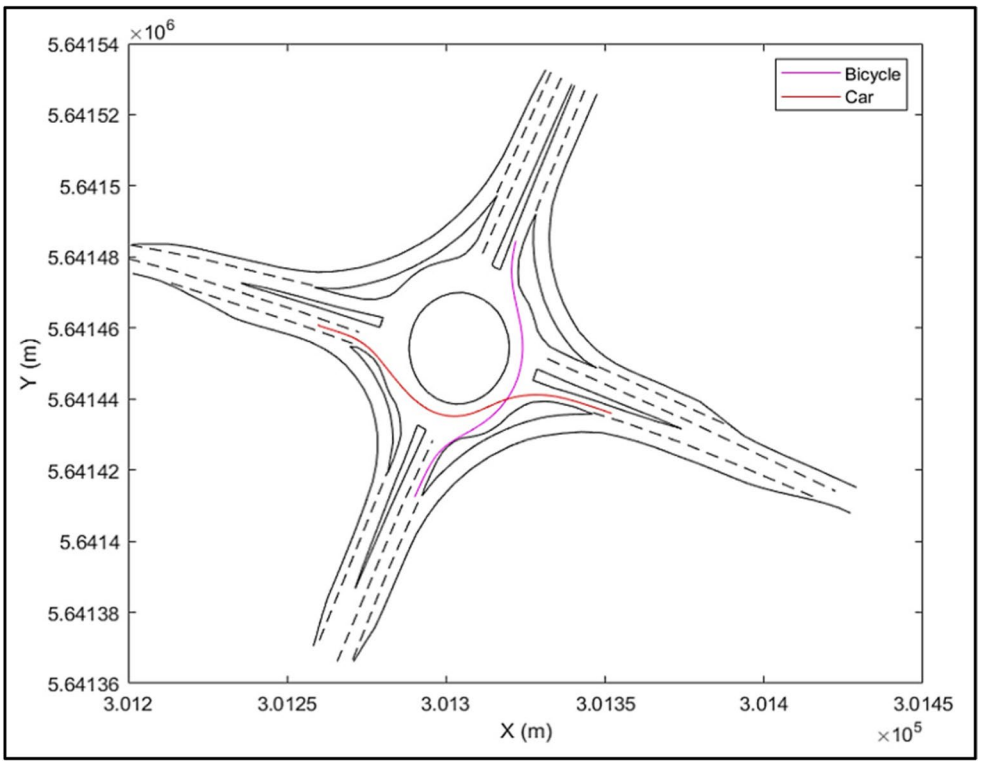

Fig. 6 Examples of bicycle and car trajectories

Fig. 7 Layout of the studied roundabout in Florida

The performance of different scenarios, including one or more forces, was analyzed to select the best resultant of forces in replicating the vehicle movement, as listed in Table 2. In the table, the Repulsive Force from other vehicles was divided into two components: the Repulsive Force from the Leading Vehicle ($\vec{F}_{vl}$ and Repulsive Force from other Surrounding Vehicles ($\vec{F}_{vs}$) to test the feasibility of ignoring the ($\vec{F}_{vl}$ in case of exerting a following force. In some scenarios (Sc6, SC7, SC8, and SC11), some forces will not be considered in case of the following behavior; otherwise, their effects will be considered.

The performance of each scenario was evaluated using the calibration data from roundabout ID1 in Germany in terms of the root mean squared error (RMSE) between the simulated and the real trajectories. The RMSE has been used in several studies to evaluate errors in trajectory prediction [12, 46, 63], and it was calculated considering the displacement between the real positions and the predicted positions from the simulation model, as formulated in Eq. (11). The positions at each time step (t + 1) were computed based on the predicted positions at time (t). However, in this study, the error is computed between the real position and the predicted one at time (t + 1), which is calculated using the real position of the vehicle at time (t) and the resultant of the forces acting on the vehicle at time (t) to avoid the accumulation of the error. In other words, the term ($\vec{x}_i(t)$) in Eq. (11) is the real vehicle position at time (t). The RMSE is calculated for each user and then averaged over all vehicles.

$$RMSE = \sqrt{\frac{\sum_i^T (x_i^s(t) - x_i^r(t))^2 + (y_i^s(t) - y_i^r(t))^2}{T}} \quad (11)$$

Table 1 Summary of the dataset used in the study

Location	Video duration (min)	# of vehicles	# of VRU	Fps	Average speed (kph)	Stage of application
ID 1 (Neuweiler)	17.88	721	11	25	29	Calibration
	18.36	666	12	25	25	Validation
	16.68	610	9	25	30	Validation
ID 2 (Kackertstraße)	17.44	324	16	25	29	Local Transferability
ID 3 (Thiergarten)	17.65	260	4	25	27	Local Transferability
UCF	20.00	462	--	30	38	External Transferability

where $(x_i^r(t), y_i^r(t))$ is the real position of vehicle (i) at time (t), $(x_i^s(t), y_i^s(t))$ is its predicted position at time (t), and T is the number of time steps.

4.3 Model Calibration

The calibration process is considered an essential step when using any simulation tool with various parameters to ensure the model's accuracy. Generally, the model comprises 18 parameters. Some parameters of the same force have different values depending on the vehicle class, such as the relaxation time, the strength, and the acting scope of the repulsive force from other vehicles; not all vehicles were treated as passenger cars. Commonly, SFMs have been calibrated using the maximum likelihood method (MLE) [12, 43, 59, 64–66] and genetic algorithm (GA) [46, 67–71]. In this study, the GA technique was adapted to search for the optimum values for the model parameters using the Genetic Algorithm toolbox embedded in MATLAB. GA is a search technique to find the best estimates of the optimization problem, which requires a fitness function to evaluate each solution. It starts using an initial population set and creates a new population at each new generation. Each set of parameters is evaluated at each iteration using the fitness function, which is the Root Mean Square Error (RMSE) of vehicle trajectories in this study, as formulated in Eq. (11).

4.4 Transferability of Model Parameters

After validating the calibrated model, the transferability of the model was evaluated using data from different environments. Generally, there are two techniques for parameters' transferability: the application-based method and the estimation-based method [72–74]. In the application-based method, the parameters calibrated using data from one location are applied to the data from the second location without any change to evaluate the performance of the calibrated model at the other location. This technique is considered easier and more direct. Nevertheless, it examines the transferability of the model as a whole without examining which specific parameters are transferable [74]. On the other hand, in the estimation-based method, the model parameters are calibrated using data from one location and then re-calibrated using the data from the second location. The transferability is conducted by investigating whether the values of the calibrated parameters differ from one location to another.

Table 2 Different simulation model scenarios

Scenario No.		$\vec{F}_d$	$\vec{F}_b$	$\vec{F}_{vs}$	$\vec{F}_{vl}$	$\vec{F}_l$	$\vec{F}_f$
SC1		✓	✓	✓	✓	✓	✓
SC2		✓	-	-	-	-	-
SC3		✓	✓	-	-	-	-
SC4		✓	✓	✓	✓	-	-
SC5		✓	✓	✓	✓	✓	-
SC6	With no following behavior	✓	✓	✓	✓	✓	-
	With the following behavior	✓	✓	✓	-	✓	✓
SC7	With no following behavior	✓	✓	✓	✓	✓	-
	With the following behavior	-	✓	✓	-	✓	✓
SC8	With no following behavior	✓	✓	✓	✓	✓	-
	With the following behavior	-	✓	✓	✓	✓	✓
SC9		✓	-	-	-	-	✓
SC10		✓	✓	-	-	✓	-
SC11	With no following behavior	✓	✓	✓	✓	✓	-
	With the following behavior	-	-	-	-	-	✓
SC12		✓	-	✓	✓	-	✓

Therefore, this technique was deemed more comprehensive as it allows the examination of the transferability of each parameter in the model [74].

Both techniques were applied in this study to assess the transferability of the model parameters to other environments. The application-based model is applied to check the performance of the calibrated model using data from different environments. If the model does not replicate the driving behavior of vehicles, the estimation-based method would be applied, and the model parameters would be recalibrated using the new dataset. The purpose of the re-calibration process in this case was to define which specific parameters are transferable. The re-calibration was conducted using the GA algorithm model with the same algorithm options applied in the first calibration process.

4.5 Model Evaluation Metrics

To evaluate the performance of the model using different datasets in the calibration, validation, and transferability process, four performance indicators were used:

- RMSE for the trajectories is computed using Eq. (11) and averaged over all vehicles.
- RMSE for the speeds is computed using the following equation:

$$RMSE_v = \sqrt{\frac{\sum_i^T (v_i^s(t) - v_i^r(t))^2}{T}} \tag{12}$$

where $v_i^s(t)$ and $v_i^r(t)$ are the simulated and real speeds of the vehicle (i) at time (t), respectively, and T is the total number of time steps.

- Final Destination Error (FDE) is calculated using Eq. (13) and averaged over all trajectories.

$$FDE = \frac{\sum_{i=1}^N \sqrt{\left(x_{i\,s}^f - x_{i\,r}^f\right)^2 + \left(y_{i\,s}^f - y_{i\,r}^f\right)^2}}{N} \tag{13}$$

where N is the number of trajectories, $(x_{i\,s}^f, y_{i\,s}^f)$ and $(x_{i\,s}^f, y_{i\,s}^f)$ are the simulated and the real final destinations of vehicle (i), respectively.

- Average Distance Error (ADE) is the average distance between the simulated and calibrated position of the vehicle at time step (t) along the whole vehicle trajectory, as shown in Eq. (14), and then averaged over the vehicles.

$$ADE = \frac{\sum_{i=1}^T \sqrt{(x_i^s(t) - x_i^r(\boldsymbol{t}))^2 + (y_i^s(\boldsymbol{t}) - y_i^r(\boldsymbol{t}))^2}}{T} \tag{14}$$

where $(x_i^s(t), y_i^s(t))$ and $(x_i^r(t), y_i^r(t))$ are the simulated and real positions of (i) at time (t), respectively, and T is the number of time steps.

Furthermore, to test the reliability of the trajectory RMSE, the bootstrapping 95% confidence interval (CI) for RMSE was computed. Boxplots were generated to visualize the error in the simulated trajectories for each vehicle type.

5 Results and Discussion

5.1 Scenario Evaluation and Model Selection

The different force combination models were applied to the calibration dataset and one validation dataset. Moreover, the percentage change in the mean difference in RMSE for all trajectories was calculated for each scenario, considering SC1 as the baseline scenario, where all the forces are included. A two-sample t-test was applied to compare the performance of each model with the baseline, with a null hypothesis that the average difference in RMSE between the two scenarios is zero. The comparison results, as well as the p-values and the 95% confidence intervals, are listed in Table 3. The table shows that ignoring the Following Force (SC 4 &5) reduced the error compared to SC1. However, adding the Following Force while ignoring the Driving Force showed the highest decrease in error (SC8). On the other hand, ignoring the Repulsive Force from the leading vehicle in the case of the Following Force (SC 6 &7) increased the RMSE in comparison to SC1, especially in the presence of the Driving Force. Therefore, SC8 was noted as the best scenario. It is noteworthy that the percentages of change in the RMSE are small because the traffic volumes at the roundabouts are low, and there are few interactions between the vehicles.

Finally, the results showed that the effects of the Following Force and the Driving Force on a vehicle (i) at the same time weakened the performance of the model. Therefore, the best model for cases with no following behavior should include the Driving Force, Repulsive Forces from other Vehicles and Boundaries, and Lane-Keeping Force, as shown in Fig. 8. Once the following behavior exists, the SFM should incorporate the Following Force instead of the Driving Force as in Fig. 8. This model was calibrated and validated in addition to testing its transferability to other datasets from various environments.

Table 3 Percentage of change in the RMSE for different force combination scenarios

Scenario No.		% Change		*P*-value Calibration data	95% CI (Calibration data)
		Calibration data	Validation dataset (ID2)		
SC1		-	-	-	-
SC2		3.610	1.605	0.00	[−0.659, −0.361]
SC3		3.610	1.135	0.02	[−0695, −0.394]
SC4		−0.045	0.043	0.278	[0.002,0.013]
SC5		−0.073	−0.056	0.198	[−0.006,0.028]
SC6	With no following behavior With the following behavior	0.018	0.006	0.119	[−0.006,0.001]
SC7	With no following behavior With the following behavior	0.106	0.015	0.07	[−2.543,0.001]
SC8	With no following behavior With the following behavior	−0.110	−0.098	0.05	[0.00, 0.242]
SC9		3.625	0.759	0.00	[−0.697, −0.396]
SC10		3.62	0.180	0.00	[−0.695, −0.394]
SC11	With no following behavior With the following behavior	−0.02	0.002	0.29	[0.005,0.210]
SC12		3.634	1.323	0.00	[−0.697, −0.396]

5.2 Model Calibration and Validation Results

The optimum values of the previously selected model parameters were calibrated using one dataset from the Neuweiler location in Germany, and the results are listed in Table 6. Figure 9 visualizes examples of simulated and real trajectories of different vehicle types, and Fig. 11 (a) shows the errors in the simulated trajectories. Moreover, the evaluation of the calibrated model in terms of the applied evaluation metrics is reported in Table 4.

The validation of the model was performed using two other datasets from the same roundabout, and the evaluation metrics are listed in Table 4. Again, the model was validated by a visual comparison of the simulated and real trajectories, as illustrated in Fig. 10, and Fig. 11 [(b), (c)] shows the errors in the simulated trajectories for each validation dataset. Hence, the model validation results showed a good performance of the calibrated model, where the simulated trajectories well-matched the real ones.

5.3 Model Transferability Evaluation

1. Local Transferability.

1 The local transferability of the validated model was evaluated by using datasets from other locations in Germany, and the evaluation results are summarized in Table 5. Additionally, the visual comparison of the simulated and real trajectories indicated strong matching, as represented in Fig. 12. Figure 13 illustrates the error in the simulated trajectories for each vehicle type using the transferability dataset. Hence, it can be concluded that the model shows good performance in describing the motion of the vehicles at other locations, even if they have different characteristics and are located in different areas. As such, the model is deemed transferable to other locations within the same country, and there was no need to conduct the estimation-based transferability approach.

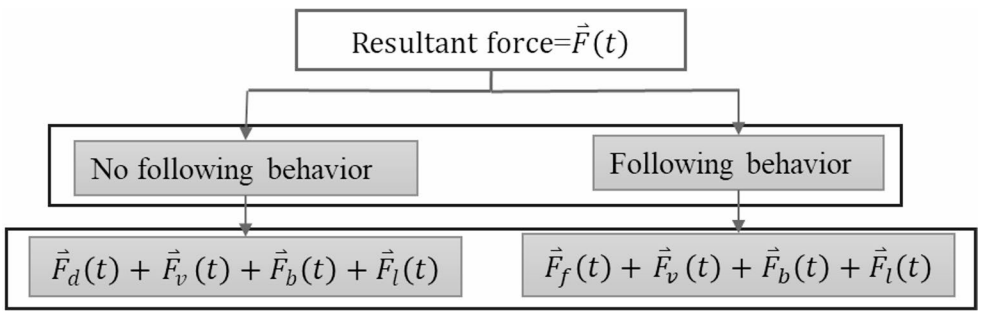

Fig. 8 The resultant force exerted on the subject vehicle at time (t)

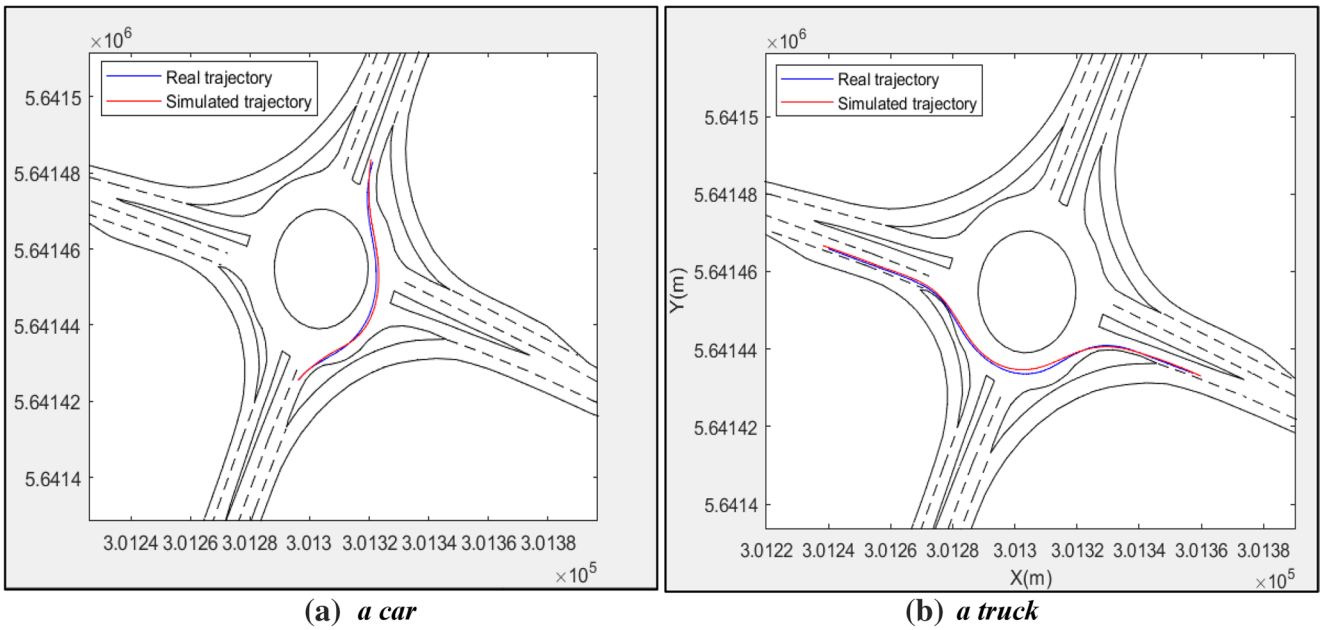

(a) ***a car*** **(b)** ***a truck***

Fig. 9 Examples of real and predicted trajectories using the dataset (1) at Location ID 1. (a) a car. (b) a truck

Table 4 Model evaluation using calibration and validation datasets

Applied dataset		$RMSE$(mean±STD)	RMSE 95% CI	$RMSE_v$(mean±STD)	ADE (m)	FDE (m)
Calibration	ID1 Dataset (1)	0.49 m±24 cm	[0.472, 0.508]	0.13 m/s± 0.1 m/s	0.30	0.78
Validation	ID1 Dataset (2)	0.35 m±34 cm	[0.329, 0.378]	0.19 m/s± 0.08 m/s	0.26	0.57
	ID1 Dataset (3)	0.55 m±30 cm	[0.528, 0.586]	0.16 m/s± 0.06 m/s	0.39	0.94

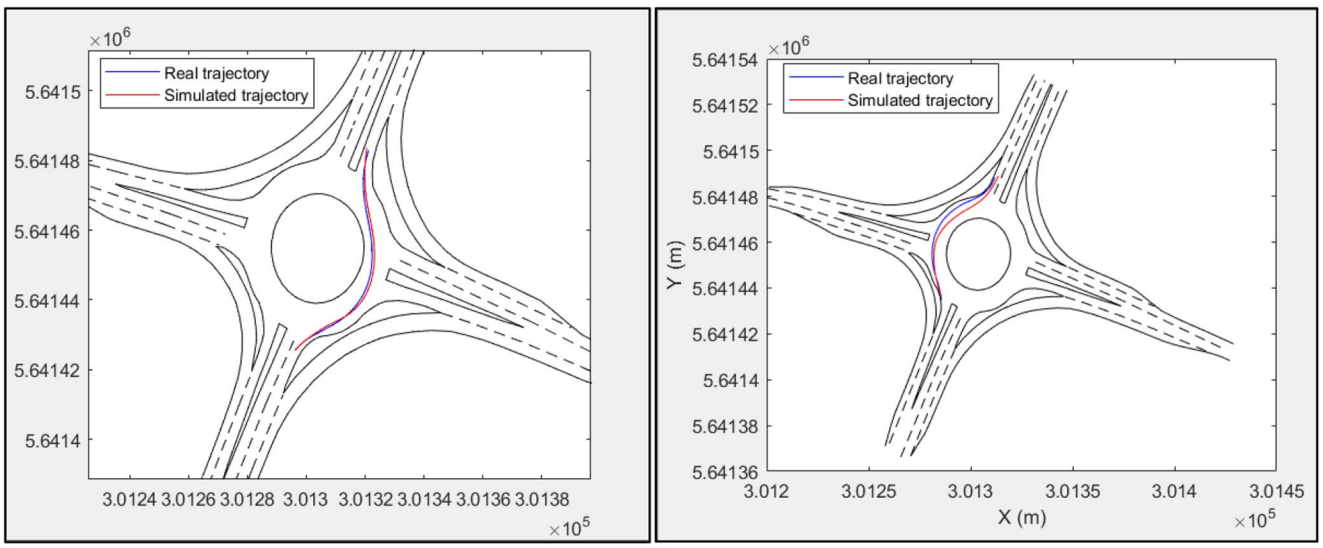

(a) ***ID 1, Dataset (2) - a car*** **(b)** ***ID1, Dataset (3) - a motorcycle***

Fig.10 A comparison between the simulated and real trajectories using the validation datasets. (**a**) ID 1, Dataset (2) - a car. (**b**) ID1, Dataset (3) - a motorcycle

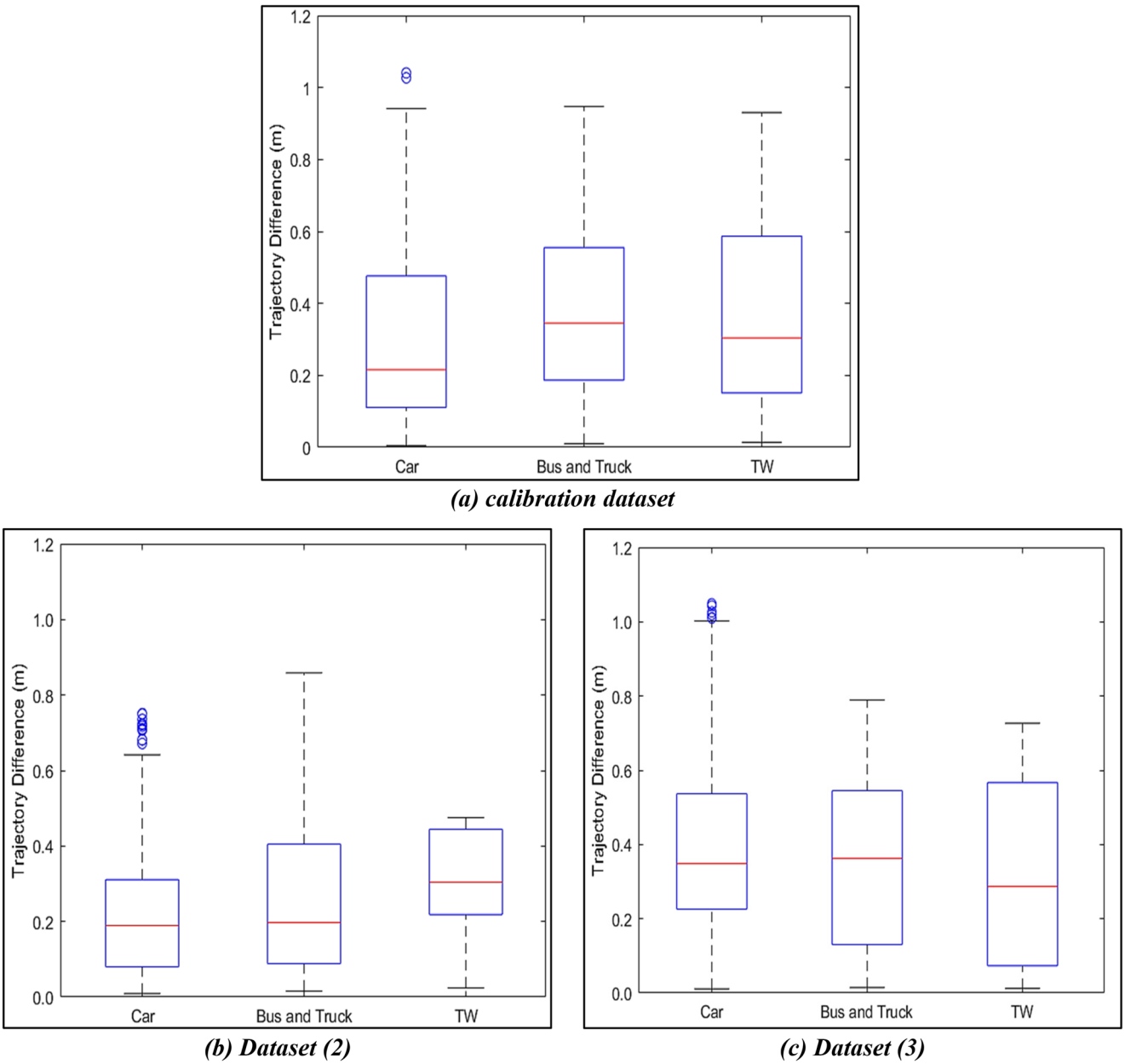

Fig. 11 Box plot of the trajectory differences for various vehicles using the validation datase. (**a**) calibration dataset. (**b**) Dataset (2). (**c**) Dataset (3)

Table 5 Model transferability evaluation results

Applied dataset		$\boldsymbol{RMSE}$ (mean ± STD)	RMSE 95% CI	$\boldsymbol{RMSE_v}$ (mean ± STD)	$\boldsymbol{ADE}$ (m)	$\boldsymbol{FDE}$ (m)
Local transferability	ID 2 Kackertstraße	0.15 m ± 18 cm	[0.128, 0.168]	$0.20\,m/s \pm 0.04\,m/s$	0.08	0.31
	ID 3 Thiergarten	0.24 m ± 20 cm	[0.210, 0.260]	$0.17\,m/s \pm 0.05\,m/s$	0.21	0.37
External transferability	Florida	0.178 m ± 9 cm	[0.171, 0.187]	$0.25\,m/s \pm 0.12\,m/s$	0.108	0.13

2 External Transferability

1 In the second stage of testing the model's transferability, the developed model was tested using a dataset from a roundabout in Florida, USA (referred to as the second location), where the application-based transferability technique was used. The simulated trajectories exhibited a significant deviation from the real ones, as shown in

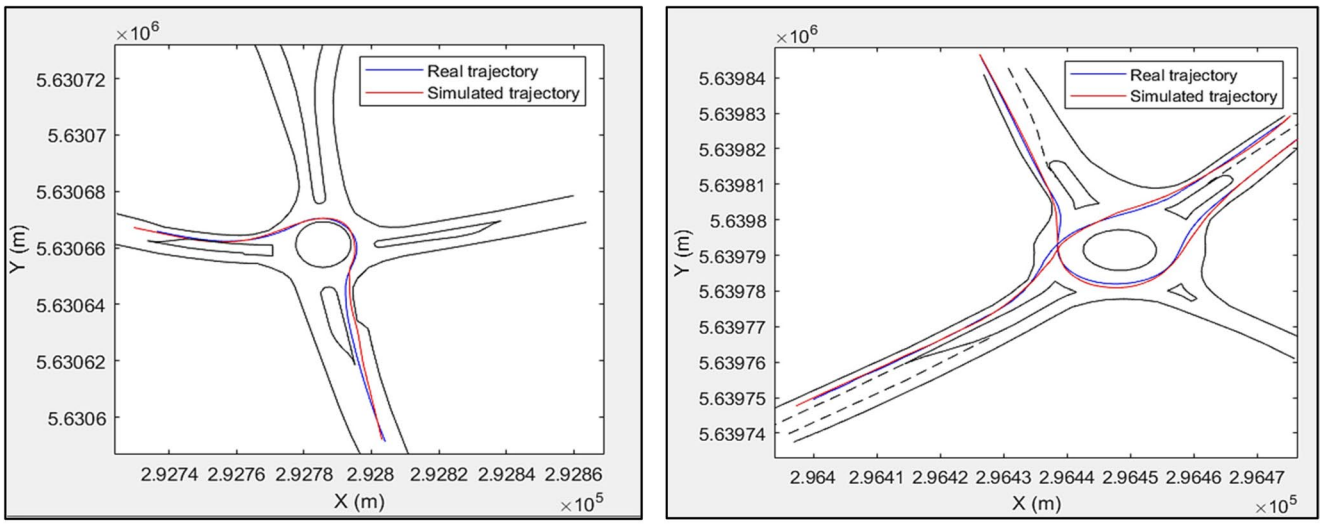

Fig. 12 Comparison between simulated and real trajectories at the other studied roundabouts in Germany. (**a**) ID2. (b) ID3

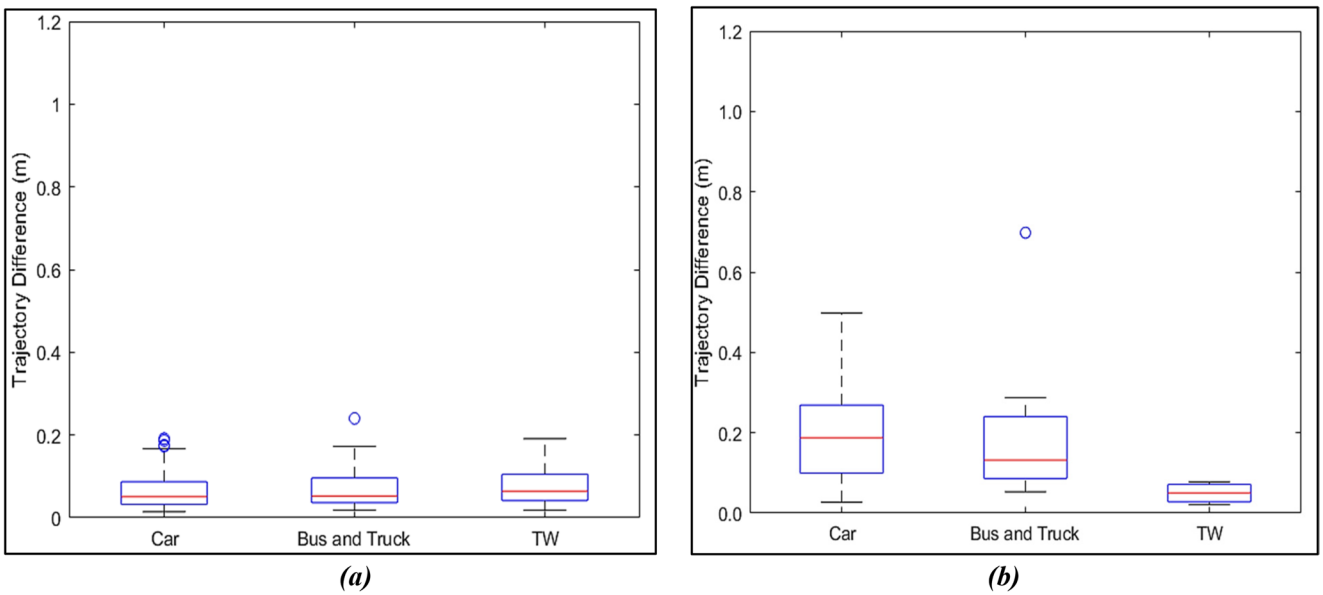

Fig. 13 Box plots of the differences in the simulated trajectories (**a**) ID2 dataset and (**b**) ID3 dataset

Fig. 14 (a). Therefore, the parameters were re-calibrated using the same GA optimization model, and the model showed a good performance in replicating the cars' movements at the roundabout, as shown in Fig. 14 (b). Moreover, the evaluation metrics were computed and presented in Table 5. Finally, the error in the simulated trajectories for each vehicle type is shown in Fig. 15.

After that, the model parameters calibrated for both the roundabouts in Germany and the one in the USA were compared to check for their similarity. The percentage of change for each parameter was computed using the following equation [74]:

$$\%\ of\ change = \frac{P_1 - P_2}{maximum\ value - minimum\ value} * 100 \quad (15)$$

where P_1, P_2 are the values of the same parameter in the two models, the maximum value is the maximum value of the parameter, and the minimum value is the minimum value of the parameter used by Zhu et al. in [75].

The calibrated values of the two models' parameters and the percentage of change are listed in Table 6. From the table, it was found that the relaxation time of the car is a transferable parameter, as there was almost no change in the values of the parameter. The percentages of change of the

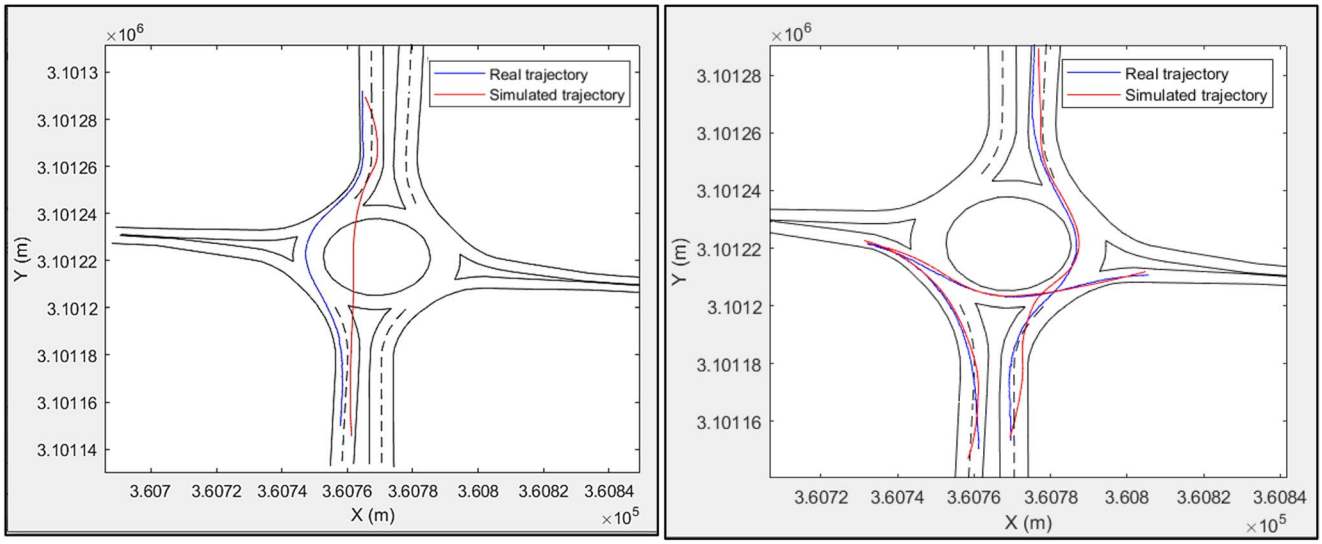

Fig. 14 An example of the simulated and real trajectories for one car at the roundabout in the USA. (**a**) Before re-calibration. (**b**) After re-calibration

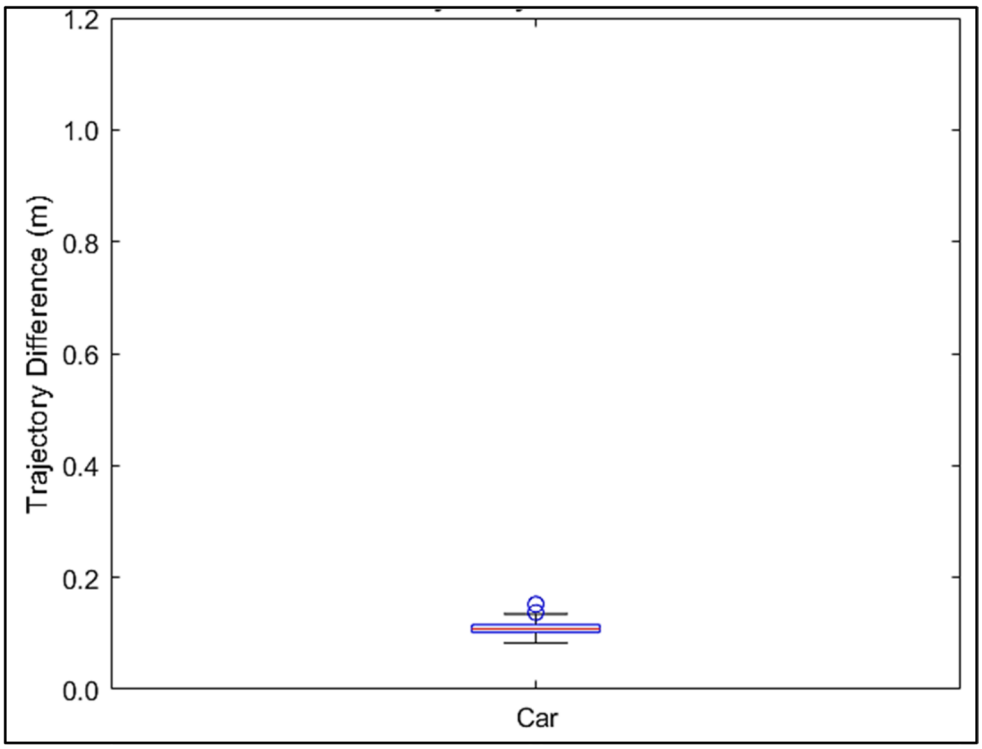

Fig. 15 Box plots of the differences in the simulated trajectories for the external transferability

acting scope of repulsive force of the car, and acting scope parameters (for a car, lane line, and boundary) are very low, which means that they are transferable. The percentage of change in the anisotropic factor was 11.26%, indicating that this parameter can also be reasonably transferable.

On the contrary, the minimum vehicle distance, the maximum deceleration of the following vehicle, the parameters representing the interaction strength of the repulsive force from the car, the boundary, and the lane line have high percentages of change. These significant differences in the interaction strength of the repulsive forces from cars and boundaries could indicate that the car drivers in Germany tend to maintain greater distances from other road users or obstacles to avoid collision than

Table 6 Calibrated values of the model parameters

Parameters		Equation	Calibrated Value		% Change
	Description		First location	Second location	
t_r	The relaxation time of the car and van (sec)	$\vec{F}_d$ (1)	0.73	0.72	0.16
	Relaxation time of the bus (sec)		1.77 *	-	-
	Relaxation time of the truck (sec)		0.46 *	-	-
	Relaxation time of the bike and motorcycle (sec)		0.51 *	-	-
A_r	Interaction strength of the repulsive force from the car (m^2/sec^2)	$\vec{F}_v$ (2)	11.72	6.26	36.37
	Interaction strength of the repulsive force from bus, truck, trailer (m^2/sec^2)		1.38 *	-	-
	Interaction strength of the repulsive force from motorcycle and bike (m^2/sec^2)		1.20 *	-	-
B_r	Acting scope of the repulsive interaction from the car (m)		3.90	4.22	−2.11
	Acting scope of the repulsive interaction from a bus or truck (m)		3.20 *	-	-
	Acting scope of the repulsive interaction from bicycle and motorcycle (m)		1.09 *	-	-
λ_i	The strength of interactions from behind (Anisotropic factor coefficient)	FoV (3)	0.40	0.51	−11.26
A_o	Strength of the repulsive force from obstacle (m/sec^2)	$\vec{F}_b$ (5)	14.25	10.80	23.03
B_o	Acting scope of boundary force (m)		2.25	1.59	4.37
A_{il}	Strength of the lane force from a lane line (m/sec^2)	$\vec{F}_l$ (6)	7.25	2.45	32.01
B_l	Acting scope of lane force (m)		1.50	0.63	5.63
α_i	Max deceleration of the following vehicle (m/sec^2)	$\vec{F}_f$ (7)	2.7	0.75	39.0
α_j	Max deceleration of the preceding vehicle (m/sec^2)		0.29	0.12	3.41
d_{min}	Minimum vehicle distance (Critical spatial distance) (m)		4.80	14.66	−69.63

*The parameter is calibrated only using data from Germany and was not included in the transferability analysis

drivers in the USA. Moreover, the value of the critical spatial difference in Germany is lower than the value in the USA due to the higher traffic volume in Germany. The traffic volume at the first location is approximately double the volume in the second one under nearly the same speeds; therefore, the distance between vehicles in the following behavior is lower. The significant differences in the values of these parameters indicate that they are not transferable and should be re-calibrated to improve the performance of the model. Noteworthy is that the traffic at the roundabout in Florida is composed of cars only, and therefore, the parameters related to the other types of vehicles were not re-calibrated, and their transferability cannot be checked.

6 Conclusions and Future Work

This study aimed to develop a social force-based simulation model to replicate the different vehicular movements at roundabouts. The implemented social force model (SFM) incorporates different forces, including a driving force, repulsive forces from other vehicles and obstacles, lane-keeping force, and following force. The performance of the model was evaluated using different datasets from several roundabouts with different attributes. Different model structures with several force scenarios were evaluated to assess the impact of ignoring one or some forces on the model's performance. It was found that the repulsive forces from other vehicles and road boundaries are essential physical forces in the SFM, while the driving force can be ignored if the following force is to be included. Generally, the proposed model included the driving force, repulsive forces, and lane-keeping force, and added the following force in cases when the following behavior exists, while ignoring the driving force.

The model was further calibrated and validated using datasets from a roundabout located in an urban area in Aachen, Germany. The validation results revealed that the proposed model can replicate the movement of various vehicles in the roundabout. The trajectory RMSE and speed RMSE were 0.35 m and 0.19 m/sec, and the final destination error (FDE) and the average distance error (ADE) were 0.57 m and 0.26 m, respectively, for the first validation dataset. Using the second validation data, the trajectory RMSE, speed RMSE, FDE, and ADE were 0.554 m, 0.16 m/sec, 0.94 m, and 0.39 m, respectively. Additionally, the local transferability of the model to other locations with

different geometric features and traffic patterns in the same city was investigated. The results showed that the model performed well at two different locations, where the RMSE of the trajectories and speeds were 0.2 m and 0.17 m/sec, respectively, at one location. At another validation location, the RMSE was 0.15 m for trajectories and 0.20 m/sec for speeds, while the FDE and ADE were 0.37 m and 0.18 m, respectively.

The external transferability of the model to another environment using a dataset from another country showed a significant deviation between the simulated and real trajectories. Therefore, the estimation-based transferability method was applied to investigate which parameters are transferable. By comparing the previously calibrated parameters with the re-calibrated values using a dataset from a roundabout in Florida, USA, it was found that the relaxation time and the acting scope parameters of the repulsive forces from vehicles, road boundaries, and lane lines are transferable. Moreover, the parameters representing the strength of repulsive forces from vehicles, boundaries, and lane lines cannot be transferred directly and should be re-calibrated. The re-calibrated model showed that the RMSE of the trajectories and speeds were 0.178 m and 0.25 m/sec m/sec, respectively, and the FDE and ADE were 0.13 m and 0.18 m, respectively. Finally, it was concluded that the developed model can represent the motion of vehicles at roundabouts after a proper calibration of the non-transferable parameters. The difference in these parameters' values reflects the difference in driving behavior in Germany and the USA, where it was shown that drivers at the studied roundabouts in Germany tend to keep more distance from other vehicles and obstacles.

The developed model is a promising initial structure to simulate the movements at traditional roundabouts using only social forces. Nonetheless, the study has some limitations that need to be tackled in future research. The behavior of pedestrians crossing and their interactions with vehicular road users at the roundabouts should be addressed. Moreover, the model can be combined with other car-following models (e.g., Intelligent Driving Model, General Motors) to investigate the most suitable car-following model for replicating the behavior at roundabouts when incorporating it with SFM. It will be a potential future research area to conduct a comparative study between the performance of this model and the other simulation models such as CA-based models and commercial microsimulation models under different traffic compositions and volumes. s While the external transferability of the model was examined on a dataset from one distinct location, it should be transferred to other locations to verify its applicability in various environments with different traffic volumes and compositions (i.e., weak lane-based roundabouts).

Declarations

Conflict of interest The authors declare that they have no known competing financial interests or personal relationships that could have appeared to influence the work reported in this paper.

References

1. Fu, L., Zhang, Y., Chen, Q., He, Y., Shen, C., Shi, Y.: Behavioral characteristics of bidirectional pedestrian-e-bike mixed flow at a signalized crosswalk: An experimental study. Travel Behav. Soc. **38**, 100897 (2025). https://doi.org/10.1016/j.tbs.2024.100897
2. Fu, L., et al.: A modified social force model for studying nonlinear dynamics of pedestrian-e-bike mixed flow at a signalized crosswalk. Chaos Solitons Fractals. **174**, 113813 (2023)
3. Gorrini, A., Crociani, L., Vizzari, G., Bandini, S.: Observation results on pedestrian-vehicle interactions at non-signalized intersections towards simulation. Transp. Res. Part. F Traffic Psychol. Behav. **59**, 269–285 (2018). https://doi.org/10.1016/j.trf.2018.09.016
4. Chen, L., Qiao, C., Zhang, J., Xie, C.-Z.T., Tang, T.-Q., Chen, Y.: Behavioral patterns of children during emergency evacuations: a comparative analysis of experimental observations and simulation results, *Journal of Statistical Mechanics: Theory and Experiment*, vol. no. 4, p. 043402, 2024, (2024). https://doi.org/10.1088/1742-5468/ad363b
5. Hamilton-Baillie, B.: Towards shared space. Urban Des. Int. **13**(2), 130–138 (2008). https://doi.org/10.1057/udi.2008.13
6. Hammond, V., Musselwhite, C.: The attitudes, perceptions and concerns of pedestrians and vulnerable road users to shared space: A case study from the UK. J. Urban Des. (Abingdon) **18**(1), 78–97 (2013). https://doi.org/10.1080/13574809.2012.739549
7. Johora, F.T., Müller, J.P.: Modeling interactions of multimodal road users in shared spaces, in *21st International Conference on Intelligent Transportation Systems (ITSC)*, IEEE, 2018, pp. 3568–3574. (2018)
8. Dias, C., Iryo-Asano, M., Nishiuchi, H., Todoroki, T.: Calibrating a social force based model for simulating personal mobility vehicles and pedestrian mixed traffic. Simulation Modelling Practice and Theory **87**, 395–411 (2018)
9. Johora, F.T., Müller, J.P.: Zone-specific interaction modeling of pedestrians and cars in shared spaces. Transportation Research Procedia **47**, 251–258 (2020)
10. Anvari, B., Bell, M.G.H., Angeloudis, P., Ochieng, W.Y.: Long-range collision avoidance for shared space simulation based on social forces. Transp. Res. Procedia. **2**, 318–326 (2014)
11. Osowski, C., Waterson, B.: The importance of interactions in determining service measures for bicycles, (2014)
12. Huang, L., Wu, J., You, F., Lv, Z., Song, H.: Cyclist social force model at unsignalized intersections with heterogeneous traffic. IEEE Trans. Industr Inf. **13**(2), 782–792 (2016)
13. Yao, J., Li, Y., He, J.: Social force model-based safety evaluation of intersections in arterials considering the pedestrian yield rule. International Journal of Environmental Research and Public Health **18**(23), 12461 (2021). https://doi.org/10.3390/ijerph182312461
14. Montella, A.: Identifying crash contributory factors at urban roundabouts and using association rules to explore their relationships to different crash types. Accid. Anal. Prev. **43**(4), 1451–1463 (2011). https://doi.org/10.1016/j.aap.2011.02.023
15. Gross, F., Lyon, C., Persaud, B., Srinivasan, R.: Safety effectiveness of converting signalized intersections to roundabouts. Accid. Anal. Prev. **50**, 234–241 (2013). https://doi.org/10.1016/j.aap.2012.04.012

16. Nikitin, N., Patskan, V., Savina, I.: Efficiency analysis of roundabout with traffic signals. Transp. Res. Procedia **20**, 443–449 (2017). https://doi.org/10.1016/j.trpro.2017.01.072
17. Li, Z., DeAmico, M., Chitturi, M.V., Bill, A.R., Noyce, D.A.: Calibration of VISSIM roundabout model: a critical gap and follow-up headway approach, in *92nd Annual Meeting of the Transportation Research Board. Washington, DC, USA*, (2013)
18. Giuffrè, T., Trubia, S., Canale, A., Persaud, B.: Using microsimulation to evaluate safety and operational implications of newer roundabout layouts for European road networks. Sustainability (2017). https://doi.org/10.3390/su9112084
19. Choi, J., Kim, D.-K.: Calibration and validation of the rule-based human driver model for car-following behaviors at roundabout using naturalistic driving data. Asian Transp. Stud. **10**, 100129 (2024). https://doi.org/10.1016/j.eastsj.2024.100129
20. Maciejewski, M.: A comparison of microscopic traffic flow simulation systems for an urban area. Transp. Probl. **5**, 27–38 (2010)
21. Board, T.R.: National academies of sciences and medicine: Roundabouts in the United States. National Academies, Washington, DC (2007). https://doi.org/10.17226/23216
22. Nikolic, G., Pringle, R., Bragg, K.: Evaluation of analytical tools used for the operational analysis of roundabouts, in *The 2010 Annual Conference of the Transportation Association of Canada*, pp. 8–10. (2010)
23. Nagel, K., Schreckenberg, M.: A cellular automaton model for freeway traffic. J. Phys. I. **2**(12), 2221–2229 (1992). https://doi.org/10.1051/jp1:1992277
24. Lakouari, N., Ez-Zahraouy, H., Benyoussef, A.: Traffic flow behavior at a single lane roundabout as compared to traffic circle. Phys. Lett. A. **378**(43), 3169–3176 (2014). https://doi.org/10.1016/j.physleta.2014.09.001
25. Wang, R., Ruskin, H.J.: Modeling traffic flow at a single-lane urban roundabout. Comput. Phys. Commun. **147**, 1–2 (2002). https://doi.org/10.1016/S0010-4655(02)00362-4
26. Echab, H., Lakouari, N., Ez-Zahraouy, H., Benyoussef, A.: Phase diagram of a single lane roundabout. Physics Letters A (2016). https://doi.org/10.1016/j.physleta.2016.01.005
27. Huang, D.: Phase diagram of a traffic roundabout. Physica A: Statistical Mechanics and its Applications **383**(2), 603–612 (2007). https://doi.org/10.1016/j.physa.2007.05.014
28. Fouladvand, M.E., Sadjadi, Z., Shaebani, M.R.: Characteristics of vehicular traffic flow at a roundabout, (2012). https://doi.org/10.1103/PhysRevE.70.046132
29. Regragui, Y., Moussa, N.: A cellular automata model for urban traffic with multiple roundabouts. Chinese Journal of Physics **56**(3), 1273–1285 (2018)
30. Wang, R., Ruskin, H.J.: Modelling traffic flow at multi-lane urban roundabouts. Int. J. Mod. Phys. C. **17**(5), 693–710 (2006). https://doi.org/10.1142/S0129183106008777
31. Bastian Schroeder, N.M., Rouphail, K., Salamati, Bugg, Z.: Effect of Pedestrian Impedance on Vehicular Capacity at Multilane Roundabouts with Consideration of Crossing Treatments, *Transp Res Rec*, vol. 2312, no. 1, pp. 14–24, Jan. (2012). https://doi.org/10.3141/2312-02
32. Regragui, Y., Moussa, N.: A cellular automata model for urban traffic with multiple roundabouts. Chin. J. Phys. **56**(3), 1273–1285 (2018). https://doi.org/10.1016/j.cjph.2018.02.010
33. Małecki, K., Wątróbski, J.: Cellular automaton to study the impact of changes in traffic rules in a roundabout: A preliminary approach. Applied Sciences (2017). https://doi.org/10.3390/app7070742
34. Liang, X., Xie, C.Z.T., Song, H.F., Guo, Y.J., Peng, J.X.: A Three-Stage cellular automata model of complex large roundabout traffic Flow, with a Flow-Efficiency- and Safety-Enhancing strategy. Sensors (2024). https://doi.org/10.3390/s24237672
35. Huang, D.W.: Modeling gridlock at roundabout. Comput. Phys. Commun. **189**, 72–76 (2015). https://doi.org/10.1016/j.cpc.2014.12.011
36. Jasti, V.K., Higgs, C.F.: A Lattice-Based cellular automata modeling approach for granular flow lubrication. J. Tribol. **128**(2), 358–364 (2005). https://doi.org/10.1115/1.2164466
37. Helbing, D., Molnar, P.: Social force model for pedestrian dynamics. Phys. Rev. E. **51**(5), 4282 (1995)
38. Fellendorf, M., Schönauer, R., Huang, W.: Social force based vehicle model for two-dimensional spaces, (2012)
39. Rinke, N., Schiermeyer, C., Pascucci, F., Berkhahn, V., Friedrich, B.: A multi-layer social force approach to model interactions in shared spaces using collision prediction. Transp. Res. Procedia. **25**, 1249–1267 (2017)
40. Li, Y., Ni, Y., Sun, J.: A modified social force model for high-density through bicycle flow at mixed-traffic intersections. Simulation Modelling Practice and Theory **108**, 102265 (2021)
41. Pascucci, F., Rinke, N., Schiermeyer, C., Friedrich, B., Berkhahn, V.: Modeling of shared space with multi-modal traffic using a multi-layer social force approach. Transportation Research Procedia **10**, 316–326 (2015)
42. Li, M., Shi, F., Chen, D.: Analyze bicycle-car mixed flow by social force model for collision risk evaluation, in *3rd International Conference on Road Safety and Simulation*, pp. 1–22. (2011)
43. Qu, Z., Cao, N., Chen, Y., Zhao, L., Bai, Q., Luo, R.: Modeling electric bike–car mixed flow via social force model. Advances in Mechanical Engineering **9**(9), 1687814017719641 (2017)
44. Johora, F.T., Müller, J.P.: Zone-specific interaction modeling of pedestrians and cars in shared spaces. Transp. Res. Procedia **47**, 251–258 (2020). https://doi.org/10.1016/j.trpro.2020.03.096
45. Johora, F.T., Müller, J.P.: Modeling interactions of multimodal road users in shared spaces, in *21st International Conference on Intelligent Transportation Systems (ITSC)*, IEEE, Nov. pp. 3568–3574. (2018). https://doi.org/10.1109/ITSC.2018.8569687
46. Johora, F.T., Müller, J.P.: On transferability and calibration of pedestrian and car motion models in shared spaces. Transportation Letters **13**(3), 172–182 (2021)
47. Yang, D., Zhou, X., Su, G., Liu, S.: Model and simulation of the heterogeneous traffic flow of the urban signalized intersection with an Island work zone. IEEE Trans. Intell. Transp. Syst. **20**(5), 1719–1727 (2018)
48. Zhu, L., et al.: Modeling the traffic flow of the urban signalized intersection with a straddling work zone, *J Adv Transp*, vol. no. 1, 2020, (2020). https://doi.org/10.1155/2020/1496756
49. Anvari, B., Daamen, W., Knoop, V.L., Hoogendoorn, S.P., Bell, M.G.H.: Shared space modeling based on social forces and distance potential field. in In: Pedestrian and Evacuation Dynamics 2012, pp. 907–916. Springer (2014)
50. Schönauer, R.: A microscopic traffic flow model for shared space. Graz Univ. Technol., (2017)
51. Dolgov, D., Thrun, S., Montemerlo, M., Diebel, J.: Path planning for autonomous vehicles in unknown semi-structured environments. Int. J. Rob. Res. **29**(5), 485–501 (2010)
52. Kurzer, K.: Path planning in unstructured environments: A real-time hybrid a* implementation for fast and deterministic path generation for the kth research concept vehicle, (2016)
53. Scharff Willners, J., Gonzalez-Adell, D., Hernández, J.D., Pairet, È., Petillot, Y.: Online 3-Dimensional path planning with kinematic constraints in unknown environments using hybrid A* with tree pruning. Sensors (2021). https://doi.org/10.3390/s21041152
54. Van Dang, C., Ahn, H., Lee, D.S., Lee, S.C.: Improved analytic expansions in hybrid a-star path planning for non-holonomic robots. Applied Sciences **12**(12), 5999 (2022)
55. Anvari, B., Bell, M.G.H., Sivakumar, A., Ochieng, W.Y.: Modelling shared space users via rule-based social force model. Transp.

Res. Part C. **51**, 83–103 (2015). https://doi.org/10.1016/j.trc.2014.10.012
56. Helbing, D., Farkas, I., Vicsek, T.: Simulating dynamical features of escape panic. Nature. **407**(6803), 487–490 (2000). https://doi.org/10.1038/35035023
57. Gipps, P.G.: A model for the structure of lane-changing decisions. Transp. Res. Part. B: Methodological. **20**(5), 403–414 (1986)
58. Yang, D., Zhou, X., Su, G., Liu, S.: Model and simulation of the heterogeneous traffic flow of the urban signalized intersection with an Island work zone. IEEE Trans. Intell. Transp. Syst. **20**(5), 1719–1727 (May 2018). https://doi.org/10.1109/TITS.2018.2834910
59. Ko, M., Kim, T., Sohn, K.: Calibrating a social-force-based pedestrian walking model based on maximum likelihood Estimation. Transp. (Amst). **40**, 91–107 (2013)
60. Krajewski, R., Moers, T., Bock, J., Vater, L., Eckstein, L.: The round dataset: A drone dataset of road user trajectories at roundabouts in germany, in *IEEE 23rd International Conference on Intelligent Transportation Systems (ITSC)*, IEEE, pp. 1–6. (2020). https://doi.org/10.1109/ITSC45102.2020.9294728
61. Zheng, O.: Development, Validation, and Integration of AI-Driven Computer Vision System and Digital-twin System for Traffic Safety Dignostics, University of Central Florida, Accessed: Jul. 16, 2025. [Online]. (2023). Available: https://stars.library.ucf.edu/etd2020/1704
62. Zheng, O., Abdel-Aty, M., Yue, L., Abdelraouf, A., Wang, Z., Mahmoud, N.: CitySim: A Drone-Based vehicle trajectory dataset for Safety-Oriented research and digital twins. Transp. Res. Rec. (2023). https://doi.org/10.48550/arXiv.2208.11036
63. Ma, W., Xie, H.: Research on multi-objective trajectory prediction algorithm based on driving intent classification, in *Journal of Physics: Conference Series*, IOP Publishing, p. 12028. (2021). https://doi.org/10.1088/1742-6596/2025/1/012028
64. Zeng, W., Chen, P., Nakamura, H., Iryo-Asano, M.: Application of social force model to pedestrian behavior analysis at signalized crosswalk. Transportation Research Part C: Emerging Technologies **40**, 143–159 (2014)
65. Daamen, W., Hoogendoorn, S.: Calibration of pedestrian simulation model for emergency doors by pedestrian type. Transp. Res. Rec. **2316**(1), 69–75 (2012). https://doi.org/10.3141/2316-08
66. Liu, M., Zeng, W., Chen, P., Wu, X.: A microscopic simulation model for pedestrian-pedestrian and pedestrian-vehicle interactions at crosswalks. PLoS One. **12**(7), e0180992 (2017). https://doi.org/10.1371/journal.pone.0180992
67. Lu, J., Dissanayake, S., Castillo, N., Williams, K.: Safety evaluation of right turns followed by u-turns as an alternative to direct left turns - Conflict analysis, (2001)
68. Evans, L.: The dominant role of driver behavior in traffic safety. Am J Public Health **86**(6), 784–786 (1996). https://doi.org/10.2105/ajph.86.6.784
69. Schiermeyer, C., Pascucci, F., Rinke, N., Berkhahn, V., Friedrich, B.: A genetic algorithm approach for the calibration of a social force based model for shared spaces, in *Proceedings of the 8th international conference on pedestrian and evacuation dynamics (PED)*, (2016)
70. Helbing, D., Farkas, I.J., Molnar, P., Vicsek, T.: Simulation of Pedestrian Crowds in Normal and Evacuation Situations, vol. 21. Springer, Berlin (2002). 2
71. Yang, D., Özgüner, Ü., Redmill, K.: A social force based pedestrian motion model considering multi-pedestrian interaction with a vehicle. ACM Transactions on Spatial Algorithms and Systems **6**(2), 1–27 (2020)
72. Sawalha, Z., Sayed, T.: Transferability of accident prediction models. Saf. Sci. **44**(3), 209–219 (2006)
73. Bowman, J.L., Bradley, M., Castiglione, J.: Making advanced travel forecasting models affordable through model transferability, (2013)
74. Sikder, S., Augustin, B., Pinjari, A.R., Eluru, N.: Spatial transferability of tour-based time-of-day choice models: Empirical assessment. Transportation Research Record: Journal of the Transportation Research Board **2429**(1), 99–109 (2014)
75. Zhu, L., et al.: Modeling the traffic flow of the urban signalized intersection with a straddling work zone. Journal of Advanced Transportation (2020). https://doi.org/10.1155/2020/1496756